This document is the accepted manuscript version of the following article:
Stadie, N. P., Wang, S., Kravchyk, K. V., & Kovalenko, M. V. (2017). Zeolite-templated carbon as an ordered microporous electrode for aluminum batteries. ACS Nano, 11(2), 1911-1919. http://doi.org/10.1021/acsnano.6b07995

Zeolite-Templated Carbon as an Ordered Microporous Electrode for Aluminum Batteries

Nicholas P. Stadie[#1,2], Shutao Wang[#1,2], Kostiantyn V. Kravchyk,[1,2] and Maksym V. Kovalenko*[1,2]

[1]Laboratory of Inorganic Chemistry, ETH Zürich, Vladimir Prelog Weg 1, CH-8093 Zürich, Switzerland

[2]Empa - Swiss Federal Laboratories for Materials Science & Technology, Überlandstrasse 129, CH-8600 Dübendorf, Switzerland

[#] These authors contributed equally to this work.

* Email: mvkovalenko@ethz.ch

KEYWORDS: aluminum, battery, ion, adsorption, porous materials, microporous, carbon, surface area, energy storage

ABSTRACT

High surface area porous carbon frameworks exhibit potential advantages over crystalline graphite as an electrochemical energy storage material owing to the possibility of faster ion transport and up to double the ion capacity, assuming a surface-based mechanism of storage. When detrimental surface-related effects such as irreversible capacity loss due to interphase formation (known as solid-electrolyte interphase, SEI) can be mitigated or altogether avoided, the greatest advantage can be achieved by maximizing the gravimetric and volumetric surface area and by tailoring the porosity to accommodate the relevant ion species. We investigate this concept by employing zeolite-templated carbon (ZTC) as the cathode in an aluminum battery based on a chloroaluminate ionic liquid electrolyte. Its ultrahigh surface area and dense, conductive network of homogeneous channels (12 Å in width) render ZTC suitable for the fast, dense storage of $AlCl_4^-$ ions (6 Å in ionic diameter). With aluminum as the anode, full cells were prepared which *simultaneously* exhibited both high specific energy (up to 64 Wh kg^{-1}, 30 Wh L^{-1}) and specific power (up to 290 W kg^{-1}, 93 W L^{-1}), highly stable cycling performance, and complete reversibility within the potential range of 0.01-2.20 V.

Table of Contents Image

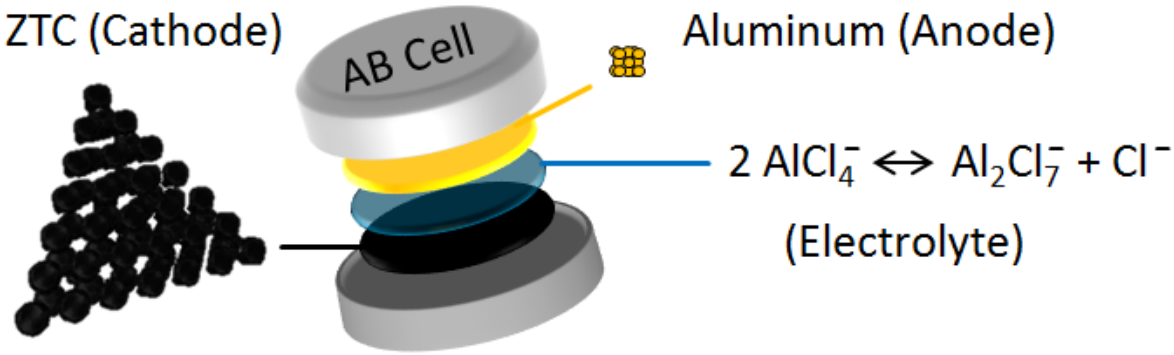

Introduction

Carbon comprises many attributes of an ideal battery electrode material due to its natural abundance, wide variety of structures and bonding motifs, robustness toward a wide range of working conditions, and tunable redox properties. In principle, it can be employed as either an anode or cathode material, by reducing (adding electrons) or oxidizing (removing electrons) during the charging step, respectively. The charge balance must then be maintained by associating the electron-rich or electron-deficient skeleton with a mobile ion of the opposite sign. Carbon materials have primarily been investigated in the context of anodic use; for example, the reduction of graphite followed by intercalation with lithium ions culminates in the formation of LiC_6, the foremost anode material for lithium-ion batteries (LIBs). The capacity of graphite as an active electrode material is, however, ultimately limited by the maximum number of ions that can be stored in each gallery between graphitic layers, i.e. on a single-sided sheet of graphene. Expanded graphite-like hard carbon structures with larger interlayer spacing can conceptually reach up to twice that capacity (as in double-sided graphene) or even more, depending on the nature (e.g., H-terminations) and relative content of edge-sites.[1-3] In sodium-ion batteries (SIBs), the intercalation of Na^+ into crystalline graphite is not possible under practical conditions, and porous hard carbons with larger interlayer spacings have therefore been a topic of active investigation as the anode material.[4-7]

A primary example of an emerging cathodic application of carbon, and also the subject of this study, is a nonaqueous battery comprising a graphitic cathode, metallic aluminum anode, and an ionic liquid chloroaluminate electrolyte.[8-11] In this report, we refer to such a battery simply as an "aluminum battery" (AB) to avoid the misconception that it is an "aluminum-ion battery", since bare Al^{3+} ions are not in fact the inserted species at the cathode. To the best of our knowledge, reversible Al^{3+} insertion has not been conclusively reported in any material, presumably due to

difficulties in diffusion caused by the high charge density of the triply-charged ions. On the contrary, when Al^{3+} is converted into $AlCl_4^-$ or $Al_2Cl_7^-$, such larger, singly-charged ions can easily be intercalated into a graphitic material upon charging (by non-destructive oxidation of the carbon structure). In this case, the electrolyte is not merely a transmitter of the active ions, as in LIBs or a hypothetical aluminum-ion battery; rather, it plays a broader role as the source of chlorine for the formation of chloroaluminate species that are then inserted into the carbon cathode (as explained in detail below).

Although functioning galvanic cells based on the three-electron redox chemistry of aluminum were first reported in 1855[12] (the first Al anode in 1857[13]), practical rechargeable batteries were not demonstrated until recently[14-15] owing to the detrimental formation of aluminum oxide films in the presence of aqueous electrolytes, and the development of suitable electrolytes for secondary ABs has been the technological crux in their realization. Thus far, the most common electrolyte for rechargeable ABs is an ionic liquid prepared by mixing $AlCl_3$ and 1-ethyl-3-methylimidazolium chloride, [EMIm]Cl, subsequently forming $AlCl_4^-$ and $Al_2Cl_7^-$ ions.[16] This can be considered a Lewis acid-base reaction leading to a "neutral melt" at a 1:1 molar mixing ratio of $AlCl_3$:[EMIm]Cl. Efficient electroplating and stripping of aluminum requires an acidic melt, i.e., an excess of $AlCl_3$. The voltage stability window of such an electrolyte is limited by the oxidative stability of the chloride ion: at potentials above 2.6 V vs. Al/Al^{3+}, it oxidizes into Cl_2. The key property of interest in such an ionic liquid AB using a carbon-based cathode is that it comprises exclusively highly abundant chemical elements, contrarily to most LIBs and SIBs which contain lithium or comparably low-abundance transition metals (Co, Ni, etc.). Aluminum and chlorine are more abundant elements in the Earth's crust than lithium (>1000 and ~10 times more, respectively) and their practical natural sources are vastly more widespread, making such ABs a possible alternative to LIBs for certain large-scale applications such as grid storage.

Graphite is a promising cathode material for ABs due to its high voltage (up to 2.45 V vs. Al/Al^{3+}) and stable capacity over thousands of cycles; however, its rather modest capacity of 60-70 mAh g^{-1} is significantly lower than that as a LIB anode (372 mAh g^{-1}), suggesting that either the larger size of the $AlCl_4^-$ ions hinders intercalation or that oxidation of graphite is less favorable than reduction. Furthermore, its capacity decreases sharply at current densities greater than ~100 mA g^{-1}.[8] Such an intercalation-type storage mechanism is expected to be slower for $AlCl_4^-$ ions than for Li^+ ions due to the former's much larger ionic radius (295 pm for $AlCl_4^-$ compared to 90 pm for Li^+)[17], a fundamental hurdle that is faced by all batteries based on the intercalation of polyatomic and/or anionic charge carriers. The slow rate capability of graphite ABs was remedied via engineering of the graphite morphology and specifically by the introduction of macroscopic voids (using ultra-low density "graphitic foam"),[8] accompanied by a reduction in bulk density of a factor of ~1000 (to ~0.005 mg mL^{-1}). Higher accessibility of the electrolyte to the interlayer space as well as significantly increased flexibility of the few-layered graphitic struts[18] were later speculated to enable the stable cycling of graphitic foam ABs at full capacity (66 mAh g^{-1}) even at extraordinary current rates up to 4 A g^{-1}.[8] However, it is also important to note that the high volumetric energy and power densities of graphite were completely forfeited upon replacement by low-density graphitic foam. It is reasonable to assume that an intermediate porous carbon material exists between bulk graphite and macroporous graphitic foam which can retain both high volumetric and gravimetric performance, while still addressing rate and capacity issues.

In an effort to improve rechargeable ABs based on $AlCl_3$ in [EMIm]Cl as the electrolyte, we propose to employ a microporous, sp^2-hybridized carbon electrode material that exhibits a high specific surface area (to ensure high gravimetric capacity) as well as the highest density of pores capable of accommodating the relevant ions (to ensure high volumetric capacity). The pore

network should be ordered and non-tortuous, to ensure high specific power, and the framework must be conductive; zeolite-templated carbon represents the closest realization of such an ideal electrode material for ABs.

Zeolite-templated carbon (ZTC) is a hard carbon material with the narrowest pore size distribution and highest density of micropores within the class of ordered porous carbons; faujasite-templated ZTC (**FAU**-ZTC) contains ~1.2 nm pores separated by molecularly thin walls across particle dimensions as large as microns.[19] Its carbon framework is conductive[20] and exhibits the highest surface area of all such materials known; however, it has largely been overlooked as an electrode material in rechargeable batteries. Early reports on the high irreversible capacity associated with ZTC-like materials[21] were consistent with the understanding that high surface area porous carbons are not suitable cathode materials for LIBs containing typical organic lithium salts as the electrolyte, due to the formation of an interphase layer that blocks the pores.[22] We consider these early, ZTC-like materials[21] not to be true ZTC since they were not adequately templated, as indicated by low specific surface areas of < 1000 m^2 g^{-1} and no demonstration of structural ordering by XRD or TEM. Therefore, it is reasonable to suggest that no thorough report of the application of ZTC as a rechargeable battery electrode material has been made to this date, although its application as an anode material in LIBs has certainly been discussed as unsuitable.[22] On the other hand, the impressive performance of fully replicate ZTC as a capacitive energy storage material has been thoroughly investigated; e.g., exhibiting a electrochemical capacitance of 300-315 F g^{-1} in aqueous electrolytes[23] and up to 240 F g^{-1} in organic electrolytes[24], showing remarkable performance even at ultrafast current rates[25] and low temperatures[26]. The highly ordered, three-connected channels of ZTC are unique among predominantly sp^2-hybridized carbonaceous materials,[19] differentiating ZTC from activated carbons (containing random pore networks and/or regions of graphitic stacking), carbide-derived

carbons[27] (containing narrower, tortuous pores and lower pore densities), and porous aromatic frameworks[28] (exhibiting conductively interrupted, sp^3-hybridized nodes).

In this work, AB cells based on microporous carbons were prepared, demonstrating a unique example of rechargeable battery electrodes based on ion insertion within a narrow, permanent microporosity comprising a high surface area for adsorption. These cells were characterized to determine the correlation between surface area and ion storage capacity in the cathode. The highest surface area material, ZTC, was found to exhibit very high capacities (up to > 380 mAh g^{-1}) in addition to high rate capabilities, even after hundreds of cycles. Further, an analysis of the energy and power density of the corresponding full-cells was performed to determine if such an increase in capacity within the cathode renders a significant improvement in performance to the overall cell. The electrolyte itself plays a large role in the charge storage mechanism(s) at play, indicating that a range of ultimate energy and power densities can be achieved; ZTC was found to enable high volumetric and gravimetric energy/power densities simultaneously, exhibiting properties intermediate between graphite and low-density graphitic foam.

Results and Discussion

Synthesis of ZTC. Samples of highly replicate zeolite-templated carbon (**FAU**-ZTC) were prepared via the impregnation of Na^+-exchanged zeolite Y (zeolite NaY, framework type code **FAU**) with furfuryl alcohol and propylene. A custom, reduced-pressure chemical vapor deposition (CVD) apparatus was used to obtain samples with both high pore-to-pore regularity and high specific surface area, and the CVD time was optimized to maximize carbon deposition within the template while reducing the undesirable deposition of carbon on the external surface. The product, heat-treated at 900 °C, cooled, freed by dissolution in HF, and dried, is referred to herein as ZTC.

The ordered structure of ZTC was confirmed primarily by X-ray powder diffraction (XRD) measurements, which show an intense reflection centered at $2\theta = 6.5°$ (d-spacing = 1.36 nm) and no intensity above background corresponding to graphitic carbon (see Figure 1a). The high intensity of the main peak, corresponding to the (111) reflection in the native zeolite template, is indicative of the highly replicate nature of ZTC.[29] A weaker (220) reflection was also observed at $2\theta = 10.6°$, further confirmation of the highly ordered nature of ZTC synthesized in this work.[30] Pore-to-pore regularity was observed in transmission electron microscopy (TEM) investigations, as demonstrated in Figure 1c-d, with a measured repeat distance of 1.4 nm. Under lower magnification, the size and shape of the ZTC particles were observed to be identical to that of the native template.

The exclusively microporous nature and exceptionally high surface area of ZTC were confirmed by investigations of N_2 adsorption at 77 K, showing a sharp knee at low pressure (below $P/P_0 = 0.2$) and a plateau at ~1000 mL_{STP} g^{-1} (see Figure 1b). This corresponds to a homogeneous pore-size distribution of ~1.2 nm in width (by non-local density functional theory (NLDFT) methods), a Dubinin-Radushkevich (DR) micropore volume of 1.40 mL g^{-1}, and a

Brunauer-Emmett-Teller (BET) surface area of > 3500 m^2 g^{-1} (see Figures S1-S3). Such an extremely high N_2 adsorption capacity can only be obtained in fully replicate ZTC with open, double-sided "blade-like" connecting structures[19] as opposed to the rarer alternate ZTC structure composed of closed, tube-like connectors[31]. Elemental analysis of ZTC by the combustion method indicated a chemical composition of approximately $C_{15}H_3O$, consistent with previous reports of fully replicate samples.[19] Altogether, the structural characterization of ZTC indicates the existence of a dense network of 1.2 nm pores organized in a cubic structure with a repeat distance of ~1.4 nm, implying the existence of molecularly thin walls and a very high surface area for adsorption.

A number of porous hard carbon materials of different pore-size and relative structural ordering were also prepared for comparison to ZTC. Zeolite-derived carbons synthesized in a similar manner to ZTC except at under-deposited CVD conditions typically exhibited slightly lower surface area (e.g., ~3370 m^2 g^{-1} for ZDC25) and reduced pore-to-pore order as indicated by weaker and broader diffraction intensity at $2\theta = 6.5°$ (see Figure S4). Over-deposited samples gave rise to dense graphitic content in the final material and were not investigated as porous electrode materials in this work. By varying the template, samples with larger ordered porosities up to ~4 nm in width were also investigated (e.g., MTC21 and MTC31, 1250-1500 m^2 g^{-1}); for consistency, furfuryl alcohol and propylene were used as the carbon precursors and the deposition temperature was maintained at 700 °C (with heat treatment at 900 °C) throughout all syntheses. Lastly, a commercially available sample of CMK-3 was obtained as a standard of reference (~650 m^2 g^{-1}, see Table S1).

ZTC as the cathode in ABs. Electrochemical cells were prepared by employing metallic aluminum as the anode, dry porous carbon as the cathode (without any binder or conductive additive), and an ionic liquid electrolyte: $AlCl_3$ in [EMIm]Cl (1.3:1 molar ratio). In direct analogy

to the corresponding graphite-based system[8-11], a simplified description of the charge storage mechanism upon charge (forward) and discharge (reverse) can be expressed as:

Anode: $$4\,Al_2Cl_7^- + 3\,e^- \leftrightarrow 7\,AlCl_4^- + Al$$ Equation 1

Cathode: $$x\,C + AlCl_4^- \leftrightarrow [AlCl_4]C_x + e^-$$ Equation 2

The theoretical capacity of graphite is reported to correspond to x = 19-21 based on this mechanism (107, 105, and 116 mAh g^{-1} at intercalation stages 4, 3, and 2, respectively).[18] This is a comparable limit to that of other polyatomic acceptor-type graphite intercalants such as BF_4^-, PF_6^-, SbF_6^-, and $[(CF_3SO_2)_2N]^-$ ($TFSI^-$), which each yield intercalation compounds corresponding to maximum charge capacities of no more than 120-140 mAh g^{-1}.[32-34] At highest capacity (stage 2, in the case of $AlCl_4^-$), this corresponds to a maximum density of one $AlCl_4^-$ ion per ~50 $Å^2$ of area on each graphene sheet facing into the intercalant gallery. Contrary to rocking-chair LIBs where the electrolyte is primarily employed as an ion conductor, the ionic liquid electrolyte in rechargeable chloroaluminate ABs acts additionally as an "active" charge storage material itself, as seen by the interconversion between $AlCl_4^-$ and $Al_2Cl_7^-$ during cycling in Equation 1.

The optimal voltage range for extended electrochemical cycling of porous carbon-based ABs was found to be 0.01-2.20 V, with two initial cycles between 0.01-2.30 V to ensure complete activation of the initially dry surface. The resulting charge/discharge capacity of the ZTC cathode is dependent on the current rate, as shown in Figure 2a. The 5th cycle capacity at 50 mA g^{-1} was 382 mAh g^{-1}, while at 1 A g^{-1} was reduced to 186 mAh g^{-1}. The voltage profile during galvanostatic cycling remained approximately the same at all current rates investigated; both charge and discharge showed capacitive (non-Faradaic) behavior without any discernible plateau, yielding an average voltage of 1.05 V.

The same surface-based behavior was observed for all the porous carbon materials investigated herein within a range of different characteristic pore size and surface area (see Figure 2b and S5). The reversible charge storage capacity of all such materials at a fixed current rate was found to be linearly dependent on surface area (e.g., 74 mAh g^{-1} discharge capacity per 1000 m^2 g^{-1} of BET surface area at a current rate of 100 mA g^{-1}, Figure S6) and did not show any particular dependence on pore size within the range investigated (1.2-4 nm). The thermochemical ionic diameter of $AlCl_4^-$ is 0.59 nm,[17] implying that pore widths of 1.2 nm and higher are not necessarily expected to give rise to significantly different effects if the bare ions are adsorbed in an unsolvated state within the pores. The highest capacity achieved (382 mAh g^{-1} in ZTC at a current rate of 50 mA g^{-1}), assuming a purely surface-based adsorption mechanism as per Equation 1, corresponds to a packing density of 2.4 monovalent ions per nm^2 (or 14.3 mmol g^{-1}). This density is slightly less than that of hexagonally close-packed spheres of 5.9 nm in diameter: 3.3 per nm^2.

The ZTC structure underwent a slight expansion upon charge/discharge cycling, as indicated by a shift in the (111) XRD reflection from $2\theta = 6.48°$ to 6.44° (a d-spacing shift of 0.1 Å, see Figure S7), but not a significant reduction in pore-to-pore order or N_2 accessible surface area. At all current rates investigated (50-1000 mA g^{-1}), cycling occurred with high coulombic efficiency (99-100%) and with excellent capacity retention over hundreds of cycles (see Figure 3). Impressively, at a current rate of 1 A g^{-1}, a capacity of 157 mAh g^{-1} was retained after 1000 cycles (86% of the initial capacity, < 0.02% loss per cycle). This corresponds to a volumetric capacity of 94 Ah L^{-1}, significantly higher than that of graphitic foam[8] which (as a cathode) exhibits < 1 Ah L^{-1} due to its ultra-low density[35]. Cells with high areal mass loadings of ZTC (up to 28 mg cm^{-2}) were also prepared to simulate a commercialized AB. In such conditions, at a rate of 100 mA g^{-1}, a capacity of 178.1 mAh g^{-1} was retained after 500 cycles and the reversible areal

capacity was 5.09 mAh cm^{-2}. The lack of any significant features in cyclic voltammetry measurements (see Figure S8) is consistent with a predominantly non-Faradaic mechanism of ion insertion in ZTC, leading to stable performance even at high current rates. The reduced capacity retention and coulombic efficiency at lower current rates can be attributed to side reactions, perhaps at oxygen-containing functionalities[19] within the ZTC or decomposition of the electrolyte.

Gravimetric energy and power densities of ZTC (as a bare cathode) in rechargeable ABs based on chloroaluminate ionic liquid electrolyte are significantly higher than those reported for graphite, despite a lower average voltage corresponding to charge and discharge (1.05 V in ZTC versus 2.0 V in graphite). A gravimetric Ragone plot (Figure 4a) demonstrates the difference between the specific energy and power for cathodes consisting of pyrolytic graphite and graphitic foam (as reported elsewhere[8]) and ZTC (this work). Graphitic foam, a material benefitting from excessive reductions in material density to overcome the slow bulk diffusion of the intercalant species, shows the highest gravimetric power performance but does not demonstrate improved specific energy over graphite or ZTC. Importantly, all gains in specific power achieved by the remarkably fast graphitic foam AB system are lost in terms of volumetric performance; a volumetric Ragone plot is shown in Figure 4b. Both the specific energy and power of graphitic foam (considering the cathode only) are reduced to values below 1 Wh L^{-1} and 10 W L^{-1}, respectively, due to its extremely low bulk density (taken herein to be 0.005 g mL^{-1}, as reported elsewhere[35]). Pyrolytic graphite, on the other hand, demonstrates the highest specific energy and power on a volumetric basis (e.g., ~100 Wh L^{-1} and ~1000 W L^{-1}), owing to its high bulk density (2.1 g mL^{-1}) and high charge/discharge potential relative to Al/Al^{3+}.

Full-cell ABs based on ZTC. The corresponding values of energy and power density for a complete working cell must be calculated based on the nominal additional mass required for the

cell body, anode, and current collectors, as well as the significant additional mass of the electrolyte. It is notable that a large proportion of the total mass of chloroaluminate-based AB cells is stored in the form of electrolyte, and the precise required amount depends on the charge/discharge reaction mechanism. The charge storage mechanism proposed in Equation 1 assumes that the only active intercalant species is $AlCl_4^-$. However, the electrolyte contains a mixture of $AlCl_4^-$, $Al_2Cl_7^-$, and free Cl^- ions,[36] of varying composition during the charging/discharging processes, and chlorine is known to form intercalation compounds with graphite (albeit slowly and typically at sub-ambient temperature or in co-intercalation conditions[37]). The starting composition of the electrolyte is determined by the ratio of $AlCl_3$ to [EMIm]Cl, r, which in this work is a fixed constant: $r = 1.3$. At equilibrium, some chloride ions will always exist in an acidic melt (when $r < 2$), expressed as:

$$2\ AlCl_4^- \leftrightarrow Al_2Cl_7^- + Cl^- \qquad \text{Equation 3}$$

The equilibrium constant of this reaction has been studied in detail for $AlCl_3$/NaCl melts at elevated temperature, in both acidic and neutral/basic conditions.[38]

Herein, we therefore address the possibility of an additional role of chloride (Cl^-) ions to the charge storage mechanism of a chloroaluminate AB cell, applicable to both graphitic- and porous carbon-based systems. Electrodeposition of aluminum can potentially occur over a range of mechanisms at the anode, and likewise the insertion of both Cl^- and $AlCl_4^-$ can be considered at the cathode, summarized as follows:

Anode: $$n\ Al_2Cl_7^- + 3\ e^- \leftrightarrow (2n-1)\ AlCl_4^- + (4-n)\ Cl^- + Al \qquad \text{Equation 4}$$

Cathode:
$$\left(x(2n-1)+y(4-n)\right)C+(2n-1)\,AlCl_4^-+(4-n)\,Cl^- \leftrightarrow (2n-1)\,[AlCl_4]C_x+(4-n)\,[Cl]C_y+(n+3)\,e^- \quad \text{Equation 5}$$

The relative role of chloride ions is expressed as "4 – n" where $4 \geq n \geq 1$: $n = 4$ corresponding to no contribution from Cl^-, and $n = 1$ corresponding to maximum contribution. The mechanism corresponding to no contribution from chloride ions ($n = 4$) is the same as that previously proposed for graphite ABs[8] (Equation 1-2). The mechanism corresponding to a large contribution from chloride ions ($n = 1$) is a variation of that reported for aluminum-chlorine rechargeable cells[39], taking into consideration the additional inclusion of $AlCl_4^-$. The parameters x and y denote the relative quantity of each ion inserted into the carbon cathode. It is directly apparent that the increasing role of Cl^- (decreasing value of n) leads to a higher number of electrons transferred per $Al_2Cl_7^-$ ion, i.e. per mass of electrolyte, leading to a very significant effect on energy/power storage density calculations in the full-cell. In order to fairly compensate for such possible effects, all calculations were performed identically for graphite- and ZTC-based ABs, based on the possibility of the range of different charge-storage mechanisms between $4 \geq n \geq 1$ (see Supporting Information for details).

Full-cell energy and power densities of graphite- and porous carbon-based ABs are presented in Figure 4, showing a non-trivial dependence of the theoretical cell capacity on the as-measured capacity of the cathode. The factor of conversion from cathode to cell depends both on the total capacity of the cathode material (increased capacity requires an increased mass of electrolyte), the average potential upon discharge, and the role of Cl^- as a charge carrier (n). Despite the low capacity of graphite, for example, the high average potential of ion insertion/removal allows less electrolyte mass to be added to the cell while still exhibiting a high overall specific energy. This effect is clearly apparent in the case of graphitic foam-based ABs where, on a volumetric basis,

cathode and cell values are almost identical (although in this case, both very low). On the other hand, large amounts of electrolyte are necessary to accommodate the high capacity of ZTC, which together with the lower average cell potential results in a larger energy/power density reduction during cathode to cell conversions. Cells consisting of densified ZTC as the cathode (at a maximum practical bulk density of 0.9 g mL^{-1}, as reported elsewhere[40]) are also shown in Figure 4 to estimate the ultimate volumetric performance for ZTC-based ABs.

Overall, ABs comprising ordered microporous carbon (ZTC) as the cathode can be seen as intermediate between those based on graphite and macroporous graphitic foam. Graphite ABs exhibit excellent energy and power density in volumetric terms, while graphitic foam cells exhibit optimal gravimetric performance (demonstrating ~10 times higher power density than ZTC-based cells). However, ZTC ABs uniquely exhibit both gravimetric (up to 64 Wh kg^{-1} at 50 mA g^{-1} and 290 W kg^{-1} at 1 A g^{-1}) and volumetric (30 Wh L^{-1} at 50 mA g^{-1} and 93 W L^{-1} at 1 A g^{-1}) capability simultaneously in a single device. Further, AB cells based on densified ZTC are estimated to exhibit even higher volumetric performance (up to 43 Wh L^{-1} at 50 mA g^{-1} and 150 W L^{-1} at 1 A g^{-1}) than graphite ABs, a factor that becomes important for portable storage applications and of less importance for stationary storage.

Further considerations. A notable difference between ZTC (or any permanently porous carbon) as the cathode in ABs and as an active electrode in LIBs and SIBs lies in the chemistry occurring at the electrode-electrolyte interface. The formation of a so-called solid-electrolyte interphase (SEI) layer on LIB and SIB anodes occurs in nearly all practically useful cell configurations and electrode-electrolyte formulations in LIBs and SIBs.[41-42] The SEI layer, with a thickness of up to ~50 nm, is Li(Na)-rich as it primarily consists of Li(Na) carbonates and alkylcarbonates.[43-45] While advantageously serving as a passivating surface layer between the electrode and the electrolyte, excessive or repetitive formation of SEI during the life of the battery can be a major

problem since every active ion (Li^+ or Na^+) incorporated into it is lost from the cathode, reducing the energy density of the cell. Clearly, the amount of SEI formed is proportional to the surface area, which has been well reported for both highly porous and nanoparticulate materials.[46-50] Therefore, porous hard carbons with large specific surface areas are not seen as a practical alternative to graphite in LIBs or dense hard carbons in SIBs[51], despite that a hypothetical strategy to increase ion capacity based on increasing surface area has been well-known for over two decades[1]. However, SEI forms primarily during the first charge as a result of reductive decomposition of the electrolyte at the anode. It is therefore a problem that is specific to the anode, and that is nearly irrelevant at the cathode, as confirmed in this work on ZTC ABs and in previous work on graphitic carbon ABs.[8-11, 52] For the high surface area carbon cathodes investigated herein, the formation of SEI, if relevant, would have been an unresolvable problem preventing continuous operation of the cell, by blocking access of the active ions to the bulk of the surface where ion storage takes place.

Conclusions

In non-SEI forming battery systems, increasing the charge storage capacity and rate capability of carbon-based electrodes is possible by utilizing designed porous structures of high surface area containing an ordered, high density of pores such as zeolite-templated carbon (ZTC). This is demonstrated herein for ionic liquid based aluminum batteries (ABs), where cells consisting of ZTC as the cathode demonstrated simultaneous volumetric and gravimetric energy storage capacities (up to 64 Wh kg^{-1} and 30 Wh L^{-1}, respectively), intermediate between graphite and graphitic foam cells which showed only one or the other. Such AB cells based on ZTC could be cycled hundreds of times without a significant loss of capacity (e.g., 0.02 % loss per cycle), an indication of the irrelevance of SEI formation to the life of the battery. The lower average voltage (~1.05 V) that results from a generally non-Faradaic charge storage mechanism does not significantly restrict the energy density of the electrode material alone, but has a significant effect on the overall energy density of the full-cell since the electrolyte acts secondarily as an active charge storage medium. Nevertheless, future secondary battery electrode concepts based on tailored, high surface area porous materials should be re-examined, especially in light of the numerous ionic liquid electrolyte battery systems of recent research interest. Lastly, future efforts to finely control the homogeneity of the pores in such materials (and therefore homogenize the ion adsorption sites) could potentially result in a more constant potential of charge/discharge, aiding in increasing the average potential of the cell and thereby the amount of energy stored.

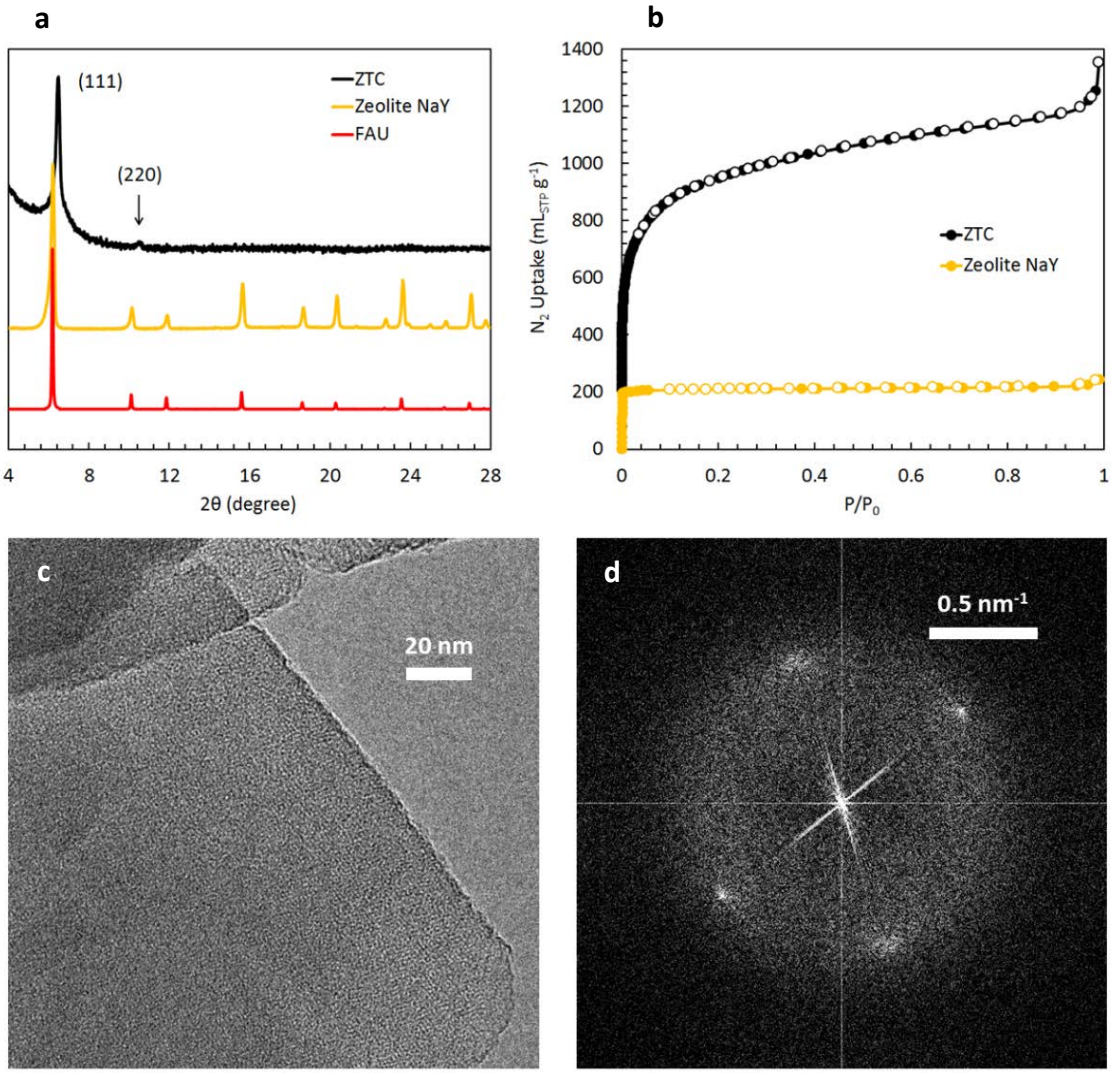

Figure 1. Ordered microporous structure of zeolite-templated carbon (ZTC). (a) X-ray diffraction pattern of ZTC (black) compared to its template (zeolite NaY, yellow) and the theoretical FAU structure (red). (b) N_2 adsorption/desorption isotherm at 77 K of ZTC (black) compared to its template (yellow). (c) Transmission electron micrograph at the edge of a typical particle of ZTC, showing distinct pore-to-pore structural order perpendicular to the edge, as confirmed by (d) the Fourier transform of the image.

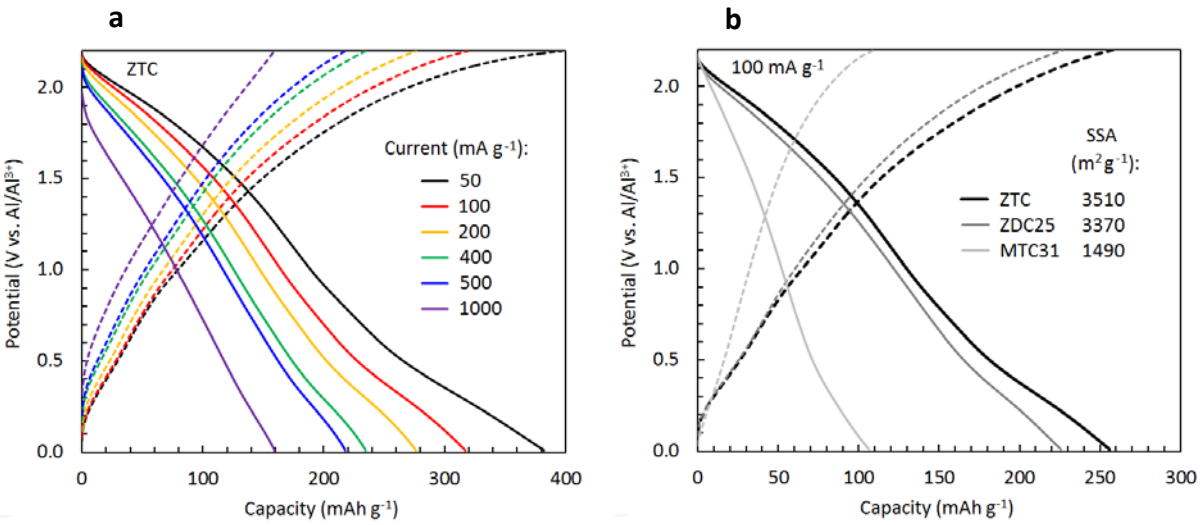

Figure 2. Electrochemical characterization of rechargeable porous carbon ABs. (a) Galvanostatic charge/discharge voltage profiles of ZTC during the 5th cycle, at current rates between 50-1000 mA g^{-1} as specified by color (discharge shown as solid lines). (b) Galvanostatic charge/discharge voltage profiles of ZTC (black), and two lower surface area porous carbon materials (dark and light gray) during the 20th cycle, at a current rate of 100 mA g^{-1}. The maximum capacity (at 0.01 V during discharge) is proportional to BET specific surface area (SSA).

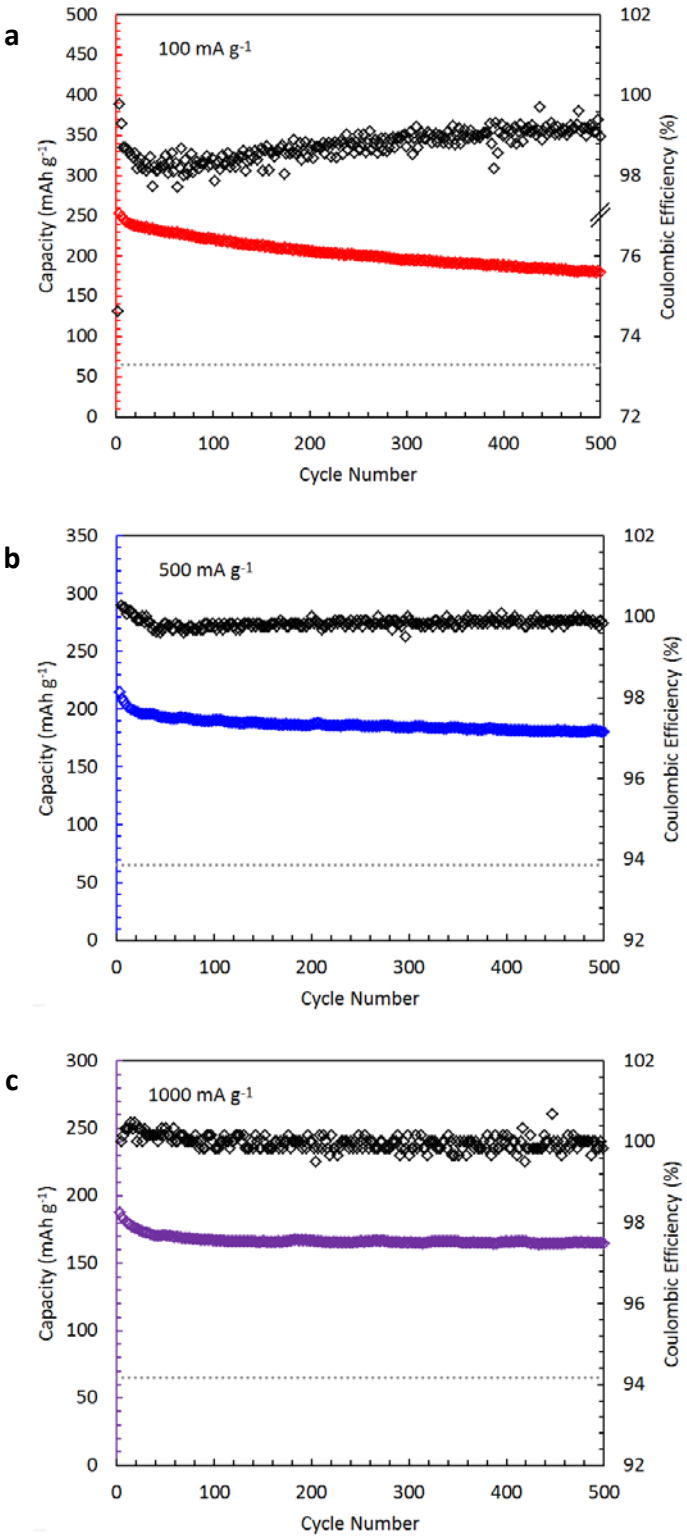

Figure 3. Discharge capacity retention (colored symbols) and coulombic efficiency (black symbols) over 500 cycles for ZTC ABs cycled between 0.01-2.20 V at various current rates: (a) 100 mA g^{-1}, (b) 500 mA g^{-1}, and (c) 1000 mA g^{-1}. For comparison, the reversible capacity of pyrolytic graphite (66 mAh g^{-1}, as reported elsewhere[8]) is also shown (dotted lines).

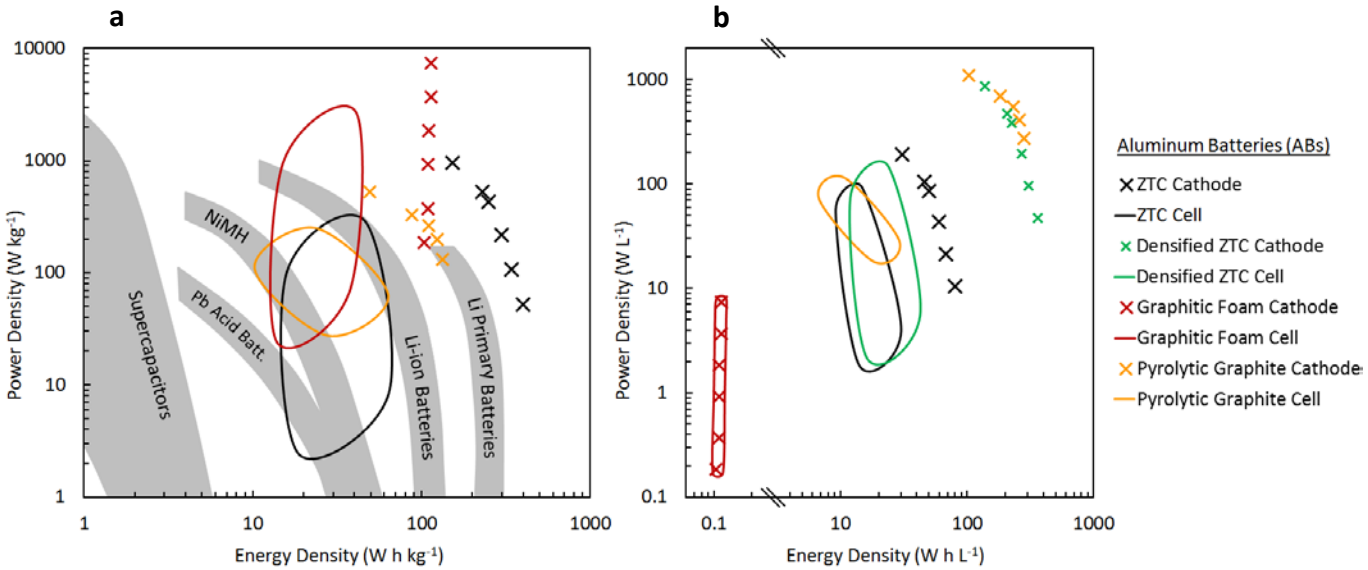

Figure 4. Ragone plots comparing various electrochemical energy storage devices (adapted from elsewhere[53]) and ABs containing ZTC (this work) and graphite (as recently reported[8]). (a) *Gravimetric* power density as a function of energy density. (b) *Volumetric* power density as a function of energy density. The amount of electrolyte needed must be known for conversions from cathode to full-cell values, which depends on the mechanism of charge storage (the entire range of mechanisms corresponding to $4 \geq n \geq 1$ are shown).

Experimental Methods

Materials Synthesis. Samples of **FAU**-ZTC were prepared according to the established two-step method[29, 54-57] via impregnation of zeolite NaY with furfuryl alcohol and then propylene as the carbon precursors. For comparison, templated carbons with either similar porosity but less pore-to-pore order (e.g., ZDC25) or larger sized, well-ordered porosity (e.g., MTC21 and MTC31) were also prepared by equivalent methods. The details of these procedures are described in Supporting Information.

Materials Characterization. Powder X-ray diffraction (XRD) measurements were performed on a STOE STADI P diffractometer in transmission geometry using Cu $K\alpha_1$ radiation (λ= 1.54 Å). Nitrogen adsorption isotherms were measured at 77 K between 10^{-3}-100 kPa using an automated volumetric instrument (BELSORP-Mini, BEL Japan Inc.). Surface areas were calculated by the Brunauer-Emmett-Teller (BET) method between P/P_0 = 0.005-0.1 and micropore volumes were calculated by the Dubinin-Radushkevich (DR) method. Pore-size distributions were determined by non-localized density functional theory (NLDFT) calculations using dedicated software (BEL-Master, BEL Japan Inc.), with a carbon slit-pore model. Transmission electron microscopy (TEM) was performed using a Tecnai TF30 microscope operated at 300 keV. Samples were prepared for TEM by dispersing a finely ground mixture of ZTC in acetone on a holey carbon grid. Thermogravimetric analysis (TGA) was performed using a Netzsch STA 409 CD instrument under argon or air flow at 40 sccm. The temperature ramp was 10 °C min^{-1} to 1200 °C. Raman spectroscopy was performed using a high-resolution confocal microscope (Ntegra Spectra, NT-MDT Inc.) equipped with a 632.8 nm HeNe laser at an incident power of 1.7 mW for excitation at room temperature. Elemental composition was determined by combustion analysis in O_2 using a LECO CHNS instrument.

Electrochemical Cell Materials. The following materials were used in the preparation of electrochemical cells: 1-ethyl-3-methylimidazolium chloride ([EMIm]Cl, >95%, BASF), $AlCl_3$ (99%, granules, Acros Organics), aluminum foil (>99.3%, 15 mm diameter, 15 μm thick, MTI Corp.), tungsten foil (0.2 mm thick, MTI Corp.), and glass microfiber discs (0.67 mm × 257 mm, GF/D grade, catalogue number 1823-257, Whatman). The as-received [EMIm]Cl was heated to 130 °C under vacuum for 32 h to remove residual water before use.

Electrolyte Preparation. The electrolyte was prepared by slowly mixing [EMIm]Cl powder and $AlCl_3$ granules under inert Ar atmosphere (<0.1 ppm H_2O/O_2) in the molar ratio of 1:1.3. A highly exothermic reaction takes place upon mixing, resulting in the formation of a light-yellow ionic liquid. This crude liquid was further treated by heating at 150 °C in the presence of Al foil for 6 h until an almost transparent, yellow ionic liquid was obtained.

Electrochemical Cell Preparation. Custom, reusable aluminum-tungsten electrochemical cells were assembled in a glovebox under inert Ar atmosphere (<0.1 ppm H_2O/O_2). Aluminum foil served as both the reference and counter electrodes. The working electrode was prepared without the use of any binder or conductive additive and the electrolyte was used as prepared above. To assemble the cell, a disc of aluminum foil was placed on the bottom of the cylindrical aluminum case and three glass microfiber discs were placed on top as the separator. The cathode material (in dry powder form) was then homogeneously distributed directly on top of the separator (at a loading of 10 mg cm^{-2}) and covered by a disc of tungsten foil. The electrolyte (200 μL) was added by wetting the exposed separator at the edge of the cell. A tungsten bar was placed on top of the tungsten disc, and finally the cell was shut, pressing all the components into contact.

Electrochemical Measurements. Cells were electrochemically cycled at 25 °C between 0.01-2.20 V on a multi-channel workstation (BST8-WA, 0.005-1 mA, up to 5 V, MTI Corp.). In certain cases, the cells were cycled between 0.01-2.30 V during the first 2 cycles to activate the

porous material. The measured charge capacities were normalized by the total initial mass of the carbon material in the cathode (since no binder or conductive additive were used). Cyclic voltammetry was also performed using a multi-channel workstation (MPG-2, Bio-Logic SAS).

Energy and Power Density Calculations. To determine the gravimetric quantities of specific energy and power of the cathode alone, the measured mass of the dry carbon material (prior to first charge) was used: typically ~4 mg. The bulk density of the ZTC cathode was measured after electrochemical cycling in the dried state: 0.2 g mL^{-1}. Conversions of cathode-specific quantities to full-cell quantities were made according to the combined mass and volume of the following components: cell casing (of nominal mass), anode, cathode, electrolyte, separator, and cathodic current collector (as detailed in Supporting Information).

Acknowledgements

We thank Frank Krumeich for assistance with TEM measurements, and Martin Kotyrba for technical assistance. This work was financially supported by the Swiss Federal Commission for Technology and Innovation (CTI) through the CTI Swiss Competence Centers for Energy Research (SCCER, "Heat and Electricity Storage") and through CTI Project Nr. 14698.2 PFIW-IW, and by the Competence Center for Energy and Mobility (CCEM, Project SLIB).

Additional Information

Synthesis details, gas adsorption, X-ray diffraction, cyclic voltammetry, and full-cell energy/power density calculations. This material is available free of charge via the Internet at http://pubs.acs.org.

Corresponding Author

*mvkovalenko@ethz.ch

Competing Financial Interests Statement

The authors declare no competing financial interests.

References

1. Dahn, J. R.; Zheng, T.; Liu, Y.; Xue, J. S., Mechanisms for Lithium Insertion in Carbonaceous Materials. *Science* **1995,** *270*, 590-593.

2. Yoo, E.; Kim, J.; Hosono, E.; Zhou, H.-s.; Kudo, T.; Honma, I., Large Reversible Li Storage of Graphene Nanosheet Families for Use in Rechargeable Lithium Ion Batteries. *Nano Lett.* **2008,** *8*, 2277-2282.

3. Wang, G.; Wang, B.; Wang, X.; Park, J.; Dou, S.; Ahn, H.; Kim, K., Sn/Graphene Nanocomposite with 3D Architecture for Enhanced Reversible Lithium Storage in Lithium Ion Batteries. *J. Mater. Chem.* **2009,** *19*, 8378-8384.

4. Doeff, M. M.; Ma, Y.; Visco, S. J.; Jonghe, L. C. D., Electrochemical Insertion of Sodium into Carbon *J. Electrochem. Soc.* **1993,** *140*, L169-L170.

5. Stevens, D. A.; Dahn, J. R., High Capacity Anode Materials for Rechargeable Sodium-Ion Batteries. *J. Electrochem. Soc.* **2000,** *147*, 1271-1273.

6. Cao, Y.; Xiao, L.; Sushko, M. L.; Wang, W.; Schwenzer, B.; Xiao, J.; Nie, Z.; Saraf, L. V.; Yang, Z.; Liu, J., Sodium Ion Insertion in Hollow Carbon Nanowires for Battery Applications. *Nano Lett.* **2012,** *12*, 3783-3787.

7. Luo, W.; Jian, Z.; Xing, Z.; Wang, W.; Bommier, C.; Lerner, M. M.; Ji, X., Electrochemically Expandable Soft Carbon as Anodes for Na-Ion Batteries. *ACS Cent. Sci.* **2015,** *1*, 516-522.

8. Lin, M.-C.; Gong, M.; Lu, B.; Wu, Y.; Wang, D.-Y.; Guan, M.; Angell, M.; Chen, C.; Yang, J.; Hwang, B.-J., et al., An Ultrafast Rechargeable Aluminium-Ion Battery. *Nature* **2015,** *520*, 324-328.

9. Sun, H.; Wang, W.; Yu, Z.; Yuan, Y.; Wang, S.; Jiao, S., A New Aluminium-Ion Battery with High Voltage, High Safety and Low Cost. *Chem. Commun.* **2015,** *51*, 11892-11895.

10. Wu, Y.; Gong, M.; Lin, M.-C.; Yuan, C.; Angell, M.; Huang, L.; Wang, D.-Y.; Zhang, X.; Yang, J.; Hwang, B.-J., et al., 3D Graphitic Foams Derived from Chloroaluminate Anion Intercalation for Ultrafast Aluminum-Ion Battery. *Adv. Mater.* **2016**, DOI: 10.1002/adma.201602958.

11. Jiao, S.; Lei, H.; Tu, J.; Zhu, J.; Wang, J.; Mao, X., An Industrialized Prototype of the Rechargeable Al/AlCl3-[EMIm]Cl/Graphite Battery and Recycling of the Graphitic Cathode into Graphene. *Carbon* **2016**, *109*, 276-281.

12. Hulot, M., Sur l'Emploi de l'Aluminium Dans La Construction Des Piles Galvaniques. *C. R. Hebd. Acad. Sci.* **1855,** *40*, 1148.

13. Tommasi, D., *Traité Théorique Et Pratique d'Électrochimie: Electrolyse, Galvanoplastie, Dorure, etc.* **1889**.

14. Jayaprakash, N.; Das, S. K.; Archer, L. A., The Rechargeable Aluminum-Ion Battery. *Chem. Commun.* **2011,** *47*, 12610-12612.

15. Paranthaman, M. P.; Brown, G. M.; Sun, X.; Nanda, J.; Manthiram, A.; Manivannan, A., A Transformational, High Energy Density Secondary Aluminum Ion Battery. *218th ECS Meeting* **2010**, Abstract 314.

16. Muldoon, J.; Bucur, C. B.; Gregory, T., Quest for Nonaqueous Multivalent Secondary Batteries: Magnesium and Beyond. *Chem. Rev.* **2014,** *114*, 11683-11720.

17. Jenkins, H. D. B.; Thakur, K. P., Reappraisal of Thermochemical Radii for Complex Ions. *Chem. Educ.* **1979,** *56*, 576-577.

18. Jung, S. C.; Kang, Y.-J.; Yoo, D.-J.; Choi, J. W.; Han, Y.-K., Flexible Few-Layered Graphene for the Ultrafast Rechargeable Aluminum-Ion Battery. *J. Phys. Chem. C* **2016**. *120* (25), 13384-13389.

19. Nishihara, H.; Yang, Q.-H.; Hou, P.-X.; Unno, M.; Yamauchi, S.; Saito, R.; Paredes, J. I.; Martínez-Alonso, A.; Tascón, J. M. D.; Sato, Y., et al., A Possible Buckybowl-Like Structure of Zeolite Templated Carbon. *Carbon* **2009,** *47*, 1220-1230.

20. Kim, K.; Lee, T.; Kwon, Y.; Seo, Y.; Song, J.; Park, J. K.; Lee, H.; Park, J. Y.; Ihee, H.; Cho, S. J., et al., Lanthanum-Catalysed Synthesis of Microporous 3D Graphene-Like Carbons in a Zeolite Template. *Nature* **2016,** *535*, 131-135.

21. Meyers, C. J.; Shah, S. D.; Patel, S. C.; Sneeringer, R. M.; Bessel, C. A.; Dollahon, N. R.; Leising, R. A.; Takeuchi, E. S., Templated Synthesis of Carbon Materials from Zeolites (Y, Beta, and ZSM-5) and a Montmorillonite Clay (K10): Physical and Electrochemical Characterization. *J. Phys. Chem. B* **2001,** *105*, 2143-2152.

22. Nishihara, H.; Kyotani, T., Templated Nanocarbons for Energy Storage. *Adv. Mater.* **2012,** *24*, 4473-4498.

23. Kajdos, A.; Kvit, A.; Jones, F.; Jagiello, J.; Yushin, G., Tailoring the Pore Alignment for Rapid Ion Transport in Microporous Carbons. *J. Am. Chem. Soc.* **2010,** *132*, 3252-3253.

24. Moon, J. S.; Kim, H.; Lee, D. C.; Lee, J. T.; Yushin, G., Increasing Capacitance of Zeolite-Templated Carbons in Electric Double Layer Capacitors. *J. Electrochem. Soc.* **2015,** *162*, A5070-A5076.

25. Itoi, H.; Nishihara, H.; Kogure, T.; Kyotani, T., Three-Dimensionally Arrayed and Mutually Connected 1.2-Nm Nanopores for High-Performance Electric Double Layer Capacitor. *J. Am. Chem. Soc.* **2011,** *133*, 1165-1167.

26. Korenblit, Y.; Kajdos, A.; West, W. C.; Smart, M. C.; Brandon, E. J.; Kvit, A.; Jagiello, J.; Yushin, G., In Situ Studies of Ion Transport in Microporous Supercapacitor Electrodes at Ultralow Temperatures. *Adv. Funct. Mater.* **2012,** *22*, 1655-1662.

27. Gogotsi, Y.; Nikitin, A.; Ye, H.; Zhou, W.; Fischer, J. E.; Yi, B.; Foley, H. C.; Barsoum, M. W., Nanoporous Carbide-Derived Carbon with Tunable Pore Size. *Nat. Mater.* **2003,** *2*, 591-594.

28. Ben, T.; Qiu, S., Porous Aromatic Frameworks: Synthesis, Structure and Functions. *CrystEngComm* **2013,** *15*, 17-26.

29. Ma, Z.; Kyotani, T.; Tomita, A., Synthesis Methods for Preparing Microporous Carbons with a Structural Regularity of Zeolite Y. *Carbon* **2002,** *40*, 2367-2374.

30. Kyakuno, H.; Matsuda, K.; Nakai, Y.; Fukuoka, T.; Maniwa, Y.; Nishihara, H.; Kyotani, T., Amorphous Water in Three-Dimensional Confinement of Zeolite-Templated Carbon. *Chem. Phys. Lett.* **2013,** *571*, 54-60.

31. Nueangnoraj, K.; Nishihara, H.; Imai, K.; Itoi, H.; Ishii, T.; Kiguchi, M.; Sato, Y.; Terauchi, M.; Kyotani, T., Formation of Crosslinked-Fullerene-Like Framework as Negative Replica of Zeolite Y. *Carbon* **2013,** *62*, 455-464.

32. Billaud, D.; Pron, A.; Vogel, F. L., Electrical Resistivity and X-Ray Spacings of Graphite Tetrafluoroborate, Hexafluorophosphate and Hexafluoroantimonate Compounds Synthesized from Nitronium Salts. *Synth. Met.* **1980,** *2*, 177-184.

33. Seel, J. A.; Dahn, J. R., Electrochemical Intercalation of Pf6 into Graphite. *J. Electrochem. Soc.* **2000,** *147*, 892-898.

34. Rothermel, S.; Meister, P.; Schmuelling, G.; Fromm, O.; Meyer, H.-W.; Nowak, S.; Winter, M.; Placke, T., Dual-Graphite Cells Based on the Reversible Intercalation of Bis(Trifluoromethanesulfonyl)Imide Anions from an Ionic Liquid Electrolyte. *Energy Environ. Sci.* **2014,** *7,* 3412-3423.

35. Chen, Z.; Ren, W.; Gao, L.; Liu, B.; Pei, S.; Cheng, H.-M., Three-Dimensional Flexible and Conductive Interconnected Graphene Networks Grown by Chemical Vapour Deposition. *Nat. Mater.* **2011,** *10*, 424-428.

36. Lai, P. K.; Skyllas-Kazacos, M., Electrodeposition of Aluminium in Aluminium Chloride/1-Methyl-3-Ethylimidazolium Chloride. *J. Electroanal. Chem.* **1988,** *248*, 431-440.

37. Hennig, G., The Properties of the Interstitial Compounds of Graphite. III. The Electrical Properties of the Halogen Compounds of Graphite. *J. Chem. Phys.* **1952,** *20*, 1443-1447.

38. Torsi, G.; Mamantov, G., Potentiometric Study of the Dissociation of the Tetrachloroaluminate Ion in Molten Sodium Chloroaluminates at 175-400°. *Inorg. Chem.* **1971,** *10*, 1900-1902.

39. Gifford, P. R.; Palmisano, J. B., An Aluminum/Chlorine Rechargeable Cell Employing a Room Temperature Molten Salt Electrolyte. *J. Electrochem. Soc.* **1988,** *135*, 650-654.

40. Hou, P.-X.; Orikasa, H.; Itoi, H.; Nishihara, H.; Kyotani, T., Densification of Ordered Microporous Carbons and Controlling Their Micropore Size by Hot-Pressing. *Carbon* **2007,** *45*, 2011-2016.

41. Verma, P.; Maire, P.; Novák, P., A Review of the Features and Analyses of the Solid Electrolyte Interphase in Li-Ion Batteries. *Electrochim. Acta* **2010,** *55*, 6332-6341.

42. Komaba, S.; Murata, W.; Ishikawa, T.; Yabuuchi, N.; Ozeki, T.; Nakayama, T.; Ogata, A.; Gotoh, K.; Fujiwara, K., Electrochemical Na Insertion and Solid Electrolyte Interphase for Hard-Carbon Electrodes and Application to Na-Ion Batteries. *Adv. Funct. Mater.* **2011,** *21*, 3859-3867.

43. Nie, M.; Chalasani, D.; Abraham, D. P.; Chen, Y.; Bose, A.; Lucht, B. L., Lithium Ion Battery Graphite Solid Electrolyte Interphase Revealed by Microscopy and Spectroscopy. *J. Phys. Chem. C* **2013,** *117*, 1257-1267.

44. Shkrob, I. A.; Zhu, Y.; Marin, T. W.; Abraham, D., Reduction of Carbonate Electrolytes and the Formation of Solid-Electrolyte Interface (Sei) in Lithium-Ion Batteries. 1. Spectroscopic Observations of Radical Intermediates Generated in One-Electron Reduction of Carbonates. *J. Phys. Chem. C* **2013,** *117*, 19255-19269.

45. Ponrouch, A.; Dedryvère, R.; Monti, D.; Demet, A. E.; Mba, J. M. A.; Croguennec, L.; Masquelier, C.; Johansson, P.; Palacín, M. R., Towards High Energy Density Sodium Ion Batteries through Electrolyte Optimization. *Energy Environ. Sci.* **2013,** *6*, 2361-2369.

46. Winter, M.; Novák, P.; Monnier, A., Graphites for Lithium-Ion Cells: The Correlation of the First-Cycle Charge Loss with the Brunauer-Emmett-Teller Surface Area. *J. Electrochem. Soc.* **1998,** *145*, 428-436.

47. Beguin, F.; Chevallier, F.; Vix-Guterl, C.; Saadallah, S.; Bertagna, V.; Rouzaud, J. N.; Frackowiak, E., Correlation of the Irreversible Lithium Capacity with the Active Surface Area of Modified Carbons. *Carbon* **2005,** *43*, 2160-2167.

48. Aricò, A. S.; Bruce, P.; Scrosati, B.; Tarascon, J.-M.; Schalkwijk, W. v., Nanostructured Materials for Advanced Energy Conversion and Storage Devices. *Nat. Mater.* **2005,** *4*, 366-377.

49. Bruce, P. G.; Scrosati, B.; Tarascon, J.-M., Nanomaterials for Rechargeable Lithium Batteries. *Angew. Chem. Int. Ed.* **2008,** *47*, 2930-2946.

50. Oszajca, M. F.; Bodnarchuk, M. I.; Kovalenko, M. V., Precisely Engineered Colloidal Nanoparticles and Nanocrystals for Li-Ion and Na-Ion Batteries: Model Systems or Practical Solutions? *Chem. Mater.* **2014,** *26*, 5422-5432.

51. Nitta, N.; Wu, F.; Lee, J. T.; Yushin, G., Li-Ion Battery Materials: Present and Future. *Mater. Today* **2015,** *18*, 252-264.

52. Hudak, N. S., Chloroaluminate-Doped Conducting Polymers as Positive Electrodes in Rechargeable Aluminum Batteries. *J. Phys. Chem. C* **2014,** *118*, 5203-5215.

53. Simon, P.; Gogotsi, Y., Materials for Electrochemical Capacitors. *Nature Materials* **2008,** *7*, 845-854.

54. Matsuoka, K.; Yamagishi, Y.; Yamazaki, T.; Setoyama, N.; Tomita, A.; Kyotani, T., Extremely High Microporosity and Sharp Pore Size Distribution of a Large Surface Area Carbon Prepared in the Nanochannels of Zeolite Y. *Carbon* **2005,** *43*, 855-894.

55. Stadie, N. P.; Vajo, J. J.; Cumberland, R. W.; Wilson, A. A.; Ahn, C. C.; Fultz, B., Zeolite-Templated Carbon Materials for High-Pressure Hydrogen Storage. *Langmuir* **2012,** *28*, 10057-10063.

56. Stadie, N. P.; Murialdo, M.; Ahn, C. C.; Fultz, B., Anomalous Isosteric Enthalpy of Adsorption of Methane on Zeolite-Templated Carbon. *J. Am. Chem. Soc.* **2013,** *135*, 990-993.

57. Nishihara, H.; Hou, P. X.; Li, L. X.; Ito, M.; Uchiyama, M.; Kaburagi, T.; Ikura, A.; Katamura, J.; Kawarada, T.; Mizuuchi, K., et al., High-Pressure Hydrogen Storage in Zeolite-Templated Carbon. *J. Phys. Chem. C* **2009,** *113*, 3189-3196.